

ULTRASONIC ASSESSMENT OF MICROCRACK DAMAGE IN CERAMICS

Y. C. Chu, M. Hefetz¹ and S. I. Rokhlin
The Ohio State University
Department of Welding Engineering
Columbus, Ohio 43210

INTRODUCTION

The inherent brittleness of ceramics often results in catastrophic failure due to microcrack damage caused by thermal treatment or mechanical loading. Extensive theoretical and experimental studies have been performed to analyze microcrack damage in ceramics caused by thermal shock [1-7]. Hasselman [1,2] proposed a simple model describing the strength behavior of ceramic materials as a function of thermal shock temperature difference ΔT . The important characteristic parameter in this model is the critical temperature difference, ΔT_c . For thermal shock temperature differences less than ΔT_c (stage I, Fig. 1) ceramics retain their strength. Thermal shocks with temperature differences equal to ΔT_c (stage II) are characterized by unstable crack propagation and instantaneous decreases in strength. Above ΔT_c is a plateau of constant strength (stage III), where cracks are subcritical and gradual decrease in strength is observed at higher thermal shock temperatures (stage IV). As shown experimentally [3,6], the actual behavior depends on the composition and the microstructure of the material.

The appearance of microcracks in the material can be considered as the appearance of a second phase, which leads to mechanical property (elastic moduli and strength) changes. The effective elastic modulus of a cracked medium depends on crack shape, density, and preferred orientation [8,9]. This makes possible ultrasonic assessment of ceramic degradation under thermal shock. This work reports on different ultrasonic techniques for assessment of damage initiation and severity. During crack nucleation and subcritical length stages (stages II and III), we use the Rayleigh critical angle method to assess damage initiation (critical temperature difference). For samples thermally shocked from higher temperatures (stage IV), we use in addition the bulk ultrasonic wave method to characterize the macroscopic elastic properties of the damaged material. The moduli measured by both techniques are compared with each other and with those predicted using damage theories.

SAMPLE PREPARATION

The materials used in the study were commercial alumina 7.5 cm diameter 0.47 cm thick discs supplied by Coors Ceramics and Si_3N_4 reaction bonded silicon nitride (RBSN) fabricated by the NASA Lewis Research Center. Alumina specimens were cut

¹now with RAFAEL, Haifa, Israel.

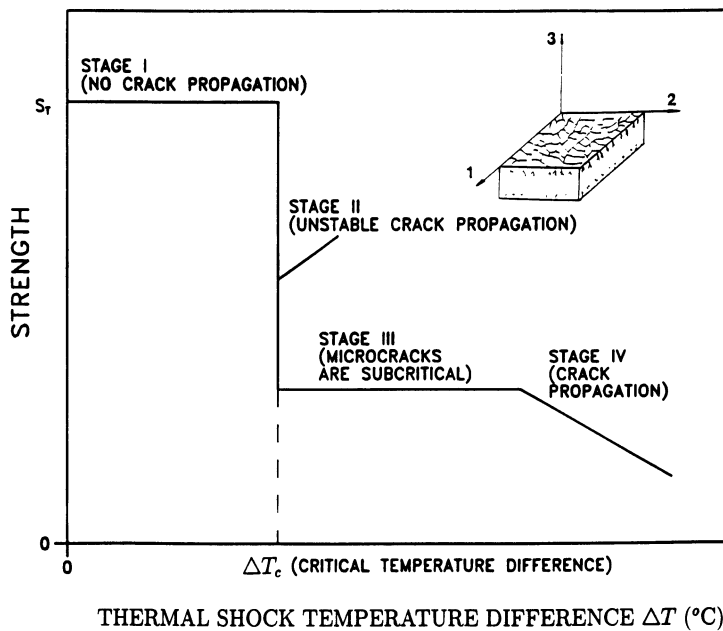


Fig. 1 Schematic representation of strength behavior as a function of severity of thermal shock as predicted by theory [1].

with a diamond blade to roughly 2.5 by 2.5 cm with thickness 4.7 mm and the RBSN specimens were cut to 12.8 by 28 mm with thickness 6.15 mm. Thermal shock treatment was done by holding the samples for at least 15 minutes in an electric furnace maintained at a predetermined temperature, and then quenching them in ice water. Different severities of thermal shock were achieved by varying the temperature of the sample before quenching in temperature ranges to 800 °C for alumina and to 1000 °C for RBSN.

DAMAGE ASSESSMENT BY RAYLEIGH CRITICAL ANGLE MEASUREMENTS

Monolithic RBSN samples were measured after thermal shocks from different elevated temperatures were measured using the Rayleigh critical angle method. The Rayleigh critical angle measurements were performed in the double reflection mode shown in Fig. 2. The ultrasonic signal is reflected by the sample surface, then by the cylindrical reflector and returned to the transducer after the second reflection from the sample surface. The amplitude of the doubly-reflected signal was recorded as a function of the rotation angle. It is known that the Rayleigh critical angle θ_R corresponds to a dip in this reflection coefficient curve (amplitude versus incident angle). The Rayleigh wave velocity V_R can be calculated via Snell's law [10]:

$$V_R = V_o / \sin \theta_R \quad (1)$$

where V_o is the sound speed in water.

We found that the reduction in the Rayleigh wave velocity due to thermal shock is very similar to the reduction in the ultimate bending strength. Fig. 3 shows the reduction in Rayleigh wave velocity and ultimate bending strength [11] in the same graph. It is noted that the ultrasonically-measured data correlate well with four-point bending tests. This means that the Rayleigh critical angle method might be useful for examining the effect of damage on the ultimate strength of ceramic materials and for determination of the critical temperature for thermal shock. It is also very important that the critical temperature corresponding to damage initiation can be determined with confidence by the ultrasonic method. For RBSN ceramics it is clear that the critical temperature for thermal shock is about 400 °C.

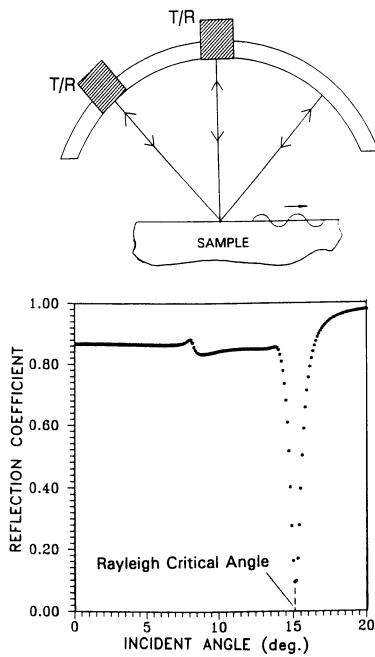


Fig. 2. Diagram of Rayleigh critical angle measurements.

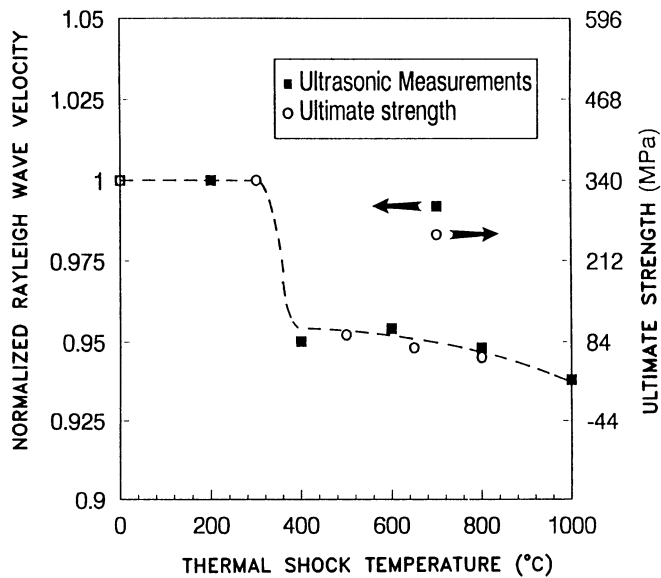


Fig. 3. Effect of thermal shock on Rayleigh wave velocities and ultimate bending strength [11] of RBSN ceramics.

It seems that for RBSN ceramics the temperature range tested corresponds to stages I to III of Hasselman's strength reduction model (Fig. 1) for thermal shock damage. Thus we conclude that the effect of damage due to thermal shock from temperatures below 1000 °C for RBSN ceramics is mainly on surface rather than bulk properties. When thermal shock temperatures increase above 1000 °C (stage IV), severe damage is expected. For Al₂O₃ all four stages may be observed using Rayleigh waves [12] in the temperature range below 800 °.

DAMAGE ASSESSMENT BY BULK ULTRASONIC WAVE MEASUREMENTS

Previous studies on thermal shock damage in alumina [2,3,12] have shown that its thermal shock critical temperature is about 200 to 300 °C and substantial growth in crack density and length begins when thermal shock temperatures are above 500 °C. To produce a uniform distribution of microcracks in the alumina sample, thermal shock temperatures were set at 600, 700 and 800 °C. Samples were evaluated after thermal shock treatment using the bulk ultrasonic wave method.

Bulk velocity measurements were performed in the double transmission mode as illustrated schematically in Fig. 4. The ultrasonic signal is transmitted through the sample, reflected by the back reflector and returned to the transducer after the second through-transmission. The measurements were performed with reference to normal incidence. This is a modification of the double-through-transmission method described by Rokhlin and Wang [13], where reference measurements were made along acoustic paths without the sample. The phase velocity at normal incidence is measured with high precision by overlapping multiple reflected signals from the front and back surfaces of the sample. The phase velocities in the samples at refraction angle θ_r (corresponding to the incident angle θ_i shown in Fig. 4) are calculated using the phase velocity in the normal direction V_n and the time delay change for the rotated sample (due to the acoustic path length change in the sample relative to that at normal incidence):

$$V_{\theta_i}(\theta_r) = \left[\frac{1}{V_n^2} + \frac{\Delta t_o - (\Delta t_o + \Delta t_{\theta_i}) \cos \theta_i}{hV_o} + \frac{\Delta t_{\theta_i}(2\Delta t_o + \Delta t_{\theta_i})}{4h^2} \right]^{-1/2} \quad (2)$$

Here V_n is the phase velocity in the samples at normal incidence, h is the thickness of the sample, $\Delta t_o = 2h(1/V_o - 1/V_n)$, and Δt_{θ_i} is the difference in the time-of-flight measurements between normal incidence and arbitrary oblique incidence at angle θ_i .

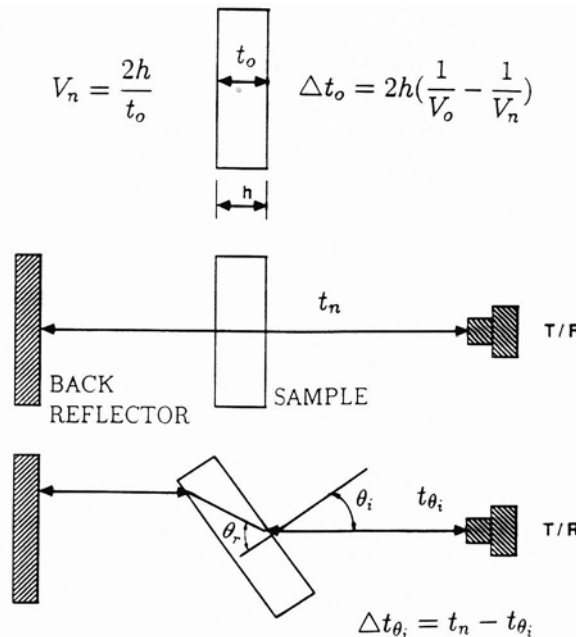


Fig. 4. Diagram of the self-reference bulk wave method.

Table 1. Effect of thermal shock damage on elastic properties of alumina samples.

Elastic properties	Without thermal shock	Thermal shock at 600 °C	Thermal shock at 700 °C	Thermal shock at 800 °C
C_{11} , GPa	453	450	427	355
C_{22} , GPa	453	450	427	355
C_{33} , GPa	453	439	446	436
C_{44} , GPa	152	136	133	127
C_{55} , GPa	152	136	133	127

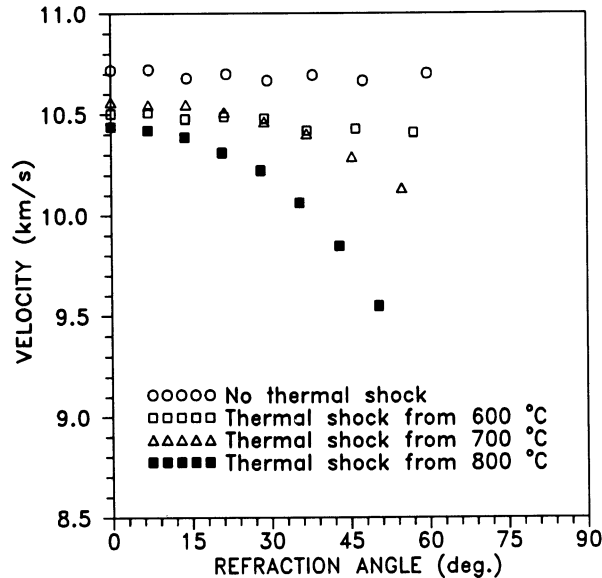


Fig. 5. Longitudinal wave velocity versus refraction angle for different thermal shock temperatures.

The longitudinal wave velocity measurements at different angles to the sample surface normal are summarized in Fig. 5. The longitudinal velocity is given versus refracted angle in the sample (angle of deviation from the sample surface normal). The data are given for different thermal shock temperatures including data for the sample without thermal shock. Strong dependence of velocity on angle of propagation can be observed in the thermal shock temperature range tested. Due to the preferred crack orientation the ultrasonic velocity in the direction normal to the sample surface is less sensitive to the damage. The velocities of waves propagating in directions near normal to the microcracks (higher refraction angle) are much more sensitive to the damage.

The elastic constants of the material have been calculated using nonlinear least square optimization [13] to obtain the best fit between the solution of the Christoffel equation and the experimentally-measured velocity. The data are summarized in Table 1 for normal and shear moduli. One can see that for damaged materials the modulus C_{33} , where the 3 axis is perpendicular to the sample surface, has only a small change, while the moduli in the plane parallel to the surface (C_{11} and C_{22}) change significantly. Thus one may infer the preferred microdamage orientation from ultrasonic data.

DAMAGE MODELING AND DETERMINATION OF MICROCRACK DENSITY

As discussed earlier ceramic microcracks caused by thermal shock treatments

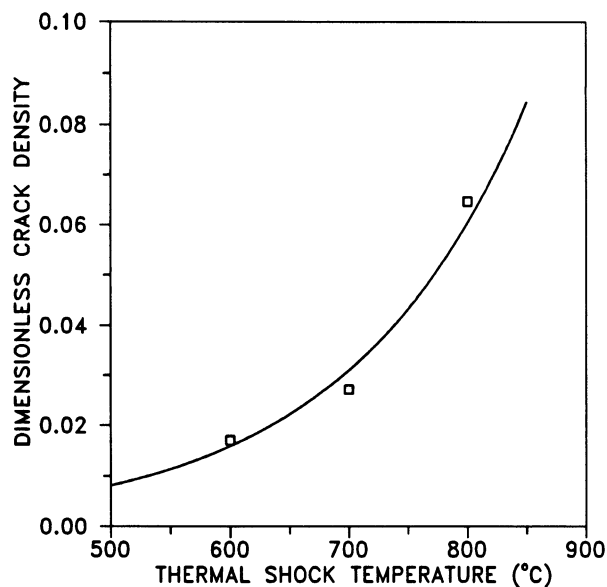


Fig. 6. The dimensionless crack density determined from ultrasonic data versus the thermal shock temperature.

are aligned normal to the sample surface. Such a preferred crack orientation allows us to assume that the microcracks in ceramic samples caused by thermal shock are two-dimensionally-oriented slit cracks. For samples with microcracks caused by thermal shock, it is reasonable to assume that the cracks are arbitrarily oriented in the 1-2 plane (but with a preferred orientation in the 3 direction). Assuming the nondamaged material is isotropic with Young's modulus E_o and Poisson's ratio ν_o , the dimensionless crack density ξ for slit cracks with width $2a$ and length l can be expressed in terms of the elastic properties of damaged and nondamaged materials [9]:

$$\xi = Na^2l = \frac{4(1 - E_t/E_o)}{\pi^2(1 - E_t\nu_o^2/E_o)} \quad (3)$$

where E_t is the transverse Young's modulus of the damaged material and N is the number of cracks per unit volume. Thus we can determine the dimensionless crack density ξ from the above equation by measuring the elastic properties with and without thermal shock.

The elastic properties of the nondamaged sample can be determined from the averaged ultrasonic velocities ($V_L=10.7$ km/s and $V_T=6.2$ km/s) and the density (3.96 g/cm³). Using the elastic properties of alumina samples after thermal shock from different temperatures (Table 1), we can calculate the dimensionless crack density corresponding to different thermal shock temperatures. The results of this calculation are shown in Fig. 6 where the dimensionless crack density is plotted as a function of thermal shock temperature. As one can see from the figure the crack density increases rapidly as the thermal shock temperature increases. This indicates increase in the number of cracks per unit volume and growth of the crack size.

The ultrasonically-measured elastic properties of cracked samples and those calculated using the damage model are shown in Figs. 7 and 8 for the transverse Young's modulus E_t and axial shear modulus G_a , respectively. In both figures the results are normalized to the moduli of the nondamaged material. The solid line is the calculated elastic modulus of the damaged material as a function of dimensionless crack density ξ using the damage model. The square points correspond to experimentally-determined transverse (to the crack surfaces) moduli of the damaged samples.

The results for the axial shear modulus obtained independently using Rayleigh

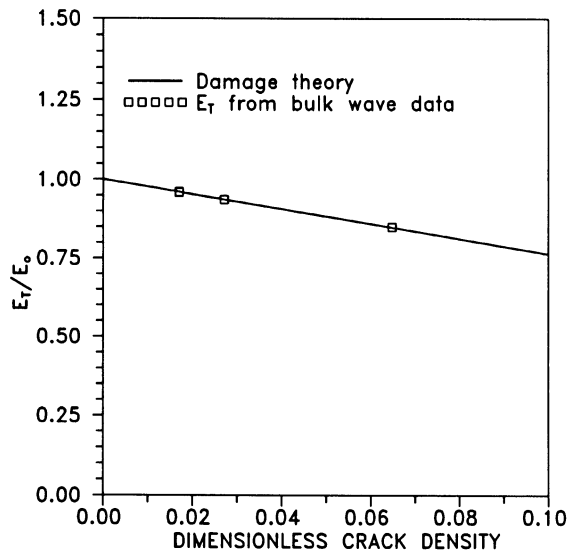


Fig. 7. Transverse Young's modulus of a damaged material versus crack density. Solid line is theory and points are experiment.

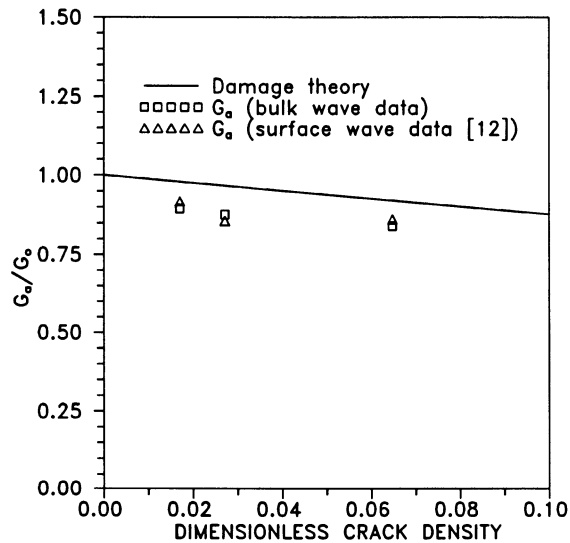


Fig. 8. Shear modulus along crack direction of a damaged material versus crack density. Solid line is theory, points are experiment (triangles correspond to the Rayleigh wave method [12] and squares to the bulk wave method).

critical angle measurements [12] are also shown in Fig. 8 (triangles). As one can see the experimental results obtained from two different measurements (bulk and Rayleigh angle methods) agree well. The ultrasonically-determined axial shear moduli behave similarly to those calculated using the damage theory but there is a systematic shift between these two at different crack densities. This difference may be due to microcrack branching, whereas the model assumes plane cracks vertically oriented.

SUMMARY

This study focuses on nondestructive assessment of microcrack damage in ceramics caused by thermal shock. Both ultrasonic bulk wave and surface wave methods have been used for assessment of thermal shock damage in ceramics. The foundation

of ultrasonic damage assessment lies in the effect of damage on elastic properties. Since the earlier stages of thermal shock damage are located near the surface, Rayleigh critical angle measurements have been found to be most appropriate for estimation of ultimate strength reduction and critical temperature of thermal shock. For severe damage caused by thermal shock (the later stages) the angular dependence of both transverse and longitudinal velocities has been found to be affected by thermal shock damage. Experimental results on two different ceramic materials show that Si_3N_4 RBSN ceramics have better thermal shock resistance than alumina. The dimensionless crack density in damaged alumina samples was determined from the reduction of elastic moduli due to thermal shock damage via an appropriate damage model. The results indicate that the crack density increases rapidly as the thermal shock temperature increases.

ACKNOWLEDGMENTS

This work was supported in part by NASA Lewis Research Center under grant #NAG3-1220. The authors appreciate Mr. Len Ewald of Coors Ceramics for supplying the alumina samples, and Dr. G. Y. Baaklini of NASA Lewis Research Center for supplying the RBSN samples.

REFERENCES

1. D. P. H. Hasselman, *J. Am. Ceram. Soc.* 52, 600 (1969).
2. D. P. H. Hasselman, *J. Am. Ceram. Soc.* 53, 490 (1970).
3. T.K. Gupta, *J. Am. Ceram. Soc.*, 55, 249 (1972).
4. A.G. Evans, *Proc. Br. Ceram. Soc.* 25, 217 (1975).
5. H.A. Bahr, G. Fischer, and H.J. Weiss, *J. Mater. Sci.* 21, 2716 (1986).
6. E. H. Lutz, M.V. Swain, and N. Claussen, *J. Am. Ceram. Soc.* 74, 19 (1991).
7. M. Oguma and T. Motomiya, *Nippon Seramikkusu Kyokai Gakujutsu Rombunshi* 97, 778 (1989).
8. B. Budiansky and R.J. O'Connell, *Int. J. Solids Structures* 12, 81 (1976).
9. N. Laws and J. R. Brockenbrough, *Int. J. Solids Structures* 23, 1247 (1987).
10. F. L. Becker and R. L. Richardson, in *Research Techniques in Nondestructive Testing*, edited by R.S. Sharpe (Academic Press, London, 1970), pp. 91.
11. R. T. Bhatt, NASA TM-101356 (1988).
12. M. Hefetz and S. I. Rokhlin, *J. Am. Ceram. Soc.* 75, 1839 (1992).
13. S.I. Rokhlin and W. Wang, *J. Acoust. Soc. Am.* 91, 3303 (1992).